Symmetry lowering at the structural phase transitions in NpO_2 and UO_2

A. V. Nikolaev* and K. H. Michel
Department of Physics, University of Antwerp, UIA, 2610 Antwerpen, Belgium
(Received 20 December 2002; revised manuscript received 19 May 2003; published 29 August 2003)

The structural phase transitions with electric-quadrupole long-range order in NpO_2 ($Fm\bar{3}m \rightarrow Pn\bar{3}m$) and UO_2 ($Fm\bar{3}m \rightarrow Pa\bar{3}$) are analyzed from a group theoretical point of view. In both cases, the symmetry lowering involves three quadrupolar components belonging to the irreducible representation T_{2g} (Γ_5) of O_h and condensing in a triple-$\vec{q}$ structure at the X point of the Brillouin zone. The $Pa\bar{3}$ structure is close to $Pn\bar{3}m$, but allows for oxygen displacements. The $Pa\bar{3}$ ordering leads to an effective electrostatic attraction between electronic quadrupoles while the $Pn\bar{3}m$ ordering results in a repulsion between them. It is concluded that the $Pn\bar{3}m$ structure can be stabilized only through some additional process such as strengthening of the chemical bonding between Np and O. We also derive the relevant structure-factor amplitudes for $Pn\bar{3}m$ and $Pa\bar{3}$, and the effect of domains on resonant x-ray scattering experiments.

DOI: 10.1103/PhysRevB.68.054112 PACS number(s): 64.70.Kb, 71.70.Ch, 75.10.Dg

I. INTRODUCTION

Since the discovery by specific-heat measurements half a century ago[1] of a phase transition in NpO_2 at a temperature $T_o = 25.5$ K, the nature of this transition in relation with magnetic and structural properties has represented a challenge for theory and experiment.[2,3] Both NpO_2 and its neighbor UO_2 (Ref. 4,5) in the actinide series have crystalline phases with cubic fluorite (CaF_2) structure at temperatures T above T_o and T_N, respectively. The temperature dependence of the magnetic susceptibility in both compounds above T_o and T_N is suggestive for a Néel transition to an antiferromagnetic state.[6,4] However, while it was found that UO_2 orders in a transverse triple-$\vec{q}$ antiferromagnetic structure at $T_N = 30.8$ K with $1.74\mu_B$/U atom,[4] no such magnetic order was detected[7,3] for NpO_2 at T_o.

The structural properties of UO_2 and NpO_2 are also different. From neutron-diffraction experiments,[8] we know that the phase transition in UO_2 is accompanied by an internal distortion of the oxygen cube that surrounds the U cation, while the external cubic structure of uranium ions survives the transition. The picture of oxygen displacements is a complex triple-$\vec{q}$ structure, which fits the $Pa\bar{3}$ space symmetry. It is characterized by magnetic moments and oxygen displacements along the four $\langle 111 \rangle$ directions.

On the other hand, no evidence for an internal or external crystallographic distortion in NpO_2 has been found by synchrotron experiments.[9] Thus, the phase transition in NpO_2 appears to be isostructural like the γ-α phase transition in elemental cerium[10,11] ($T_c \sim 100$ K) or the isostructural expansion in $YbInCu_4$ at $T_c = 42$ K.[12] It is worth mentioning that in all these compounds, the phase transition is accompanied by a loss of magnetic moments in the ordered phase.

To describe the disappearance of magnetic moments of Np at $T < T_o$, Santini and Amoretti put forward the idea of a magnetic octupole order parameter,[13] which on one hand, is not invariant under time-reversal symmetry and, on the other hand, is different from the magnetic dipolar order parameter which brings about the ordinary magnetic ordering. The idea of breaking down of Kramers' degeneracy by the magnetic octupole seems to be the only solution in the framework of the $5f^3$ model.[3,13]

An important progress in elucidating the puzzling nature of the phase transition in NpO_2 was provided by recent resonant x-ray scattering (RXS) experiments[14] at the Np M_{IV} and M_V absorption edges. While earlier RXS experiments[9] were interpreted in terms of an unusual triple-$\vec{q}$ magnetic structure, it later became clear by polarization analysis of the diffraction radiation that the superlattice peaks in NpO_2 are not magnetic but signal the occurrence of electric quadrupole long-range order with space-group symmetry $Pn\bar{3}m$ below T_o. It was pointed out in Ref. 13 that quadrupolar order alone is not sufficient as it cannot explain the absence of a disordered magnetic moment and the breaking of invariance under time-reversal. The breaking of time reversal symmetry below T_o is demonstrated by muon spin-relaxation experiments.[15] Hence, the authors of Ref. 14 infer the existence of an octupolar magnetic order parameter[13] (OP) which transforms as the irreducible representation Γ_5 (T_{2u}) of O_h. It is suggested[14] that this octupolar OP induces the observed triple-$\vec{q}$ structure of Γ_5 (T_{2g}) quadrupoles as secondary OP. We observe that the relation between electric quadrupolar order and accompanying structural phase transitions with lattice deformations and change of magnetic properties is a problem of current research. In particular, it has been suggested[16] that the γ-α transition[10] in Ce is driven by electric quadrupolar ordering with $Pa\bar{3}$ symmetry. The experimental verification of this hypothesis is still open.

In the present paper, we will investigate from a group theoretical point of view the electric quadrupole-quadrupole interactions on a fcc lattice. We will discuss the order parameter and condensation schemes that lead to the $Pa3$ and $Pn3m$ structures, and study the corresponding quadrupolar interaction energies. Since the space groups $Pa3$ and $Pn3m$ are variants of triple-$\vec{q}^X$ ordering and since both symmetries are very similar, we will give a detailed discussion of the corresponding RXS scattering laws and domain structures.

II. STRUCTURAL PHASE TRANSITIONS AND SYMMETRY LOWERING

The crystal structure in the high-T phases ($T>T_o$ and $T>T_N$, respectively) has the cubic space group $Fm\bar{3}m$ and the site point group is O_h. The electron-density distribution of Np or U ions on the face-centered-cubic lattice has full cubic symmetry. Deviations from spherical symmetry are described by the cubic harmonics $K_l(\Omega)$, $\Omega=(\Theta,\phi)$, $l=4,6,\ldots$. [Here Ω stands for the polar angles (Θ,ϕ).] The cubic harmonics have the unit symmetry (A_{1g}) of O_h. There is no contribution from quadrupolar functions $Y^{\alpha}_{l=2}$, where $\alpha=(m,c)$ or (m,s):

$$Y_l^{(m,c)}(\Omega)=\frac{1}{\sqrt{2}}[Y_l^m(\Omega)+Y_l^{-m}(\Omega)], \tag{2.1a}$$

$$Y_l^{(m,s)}(\Omega)=-\frac{i}{\sqrt{2}}[Y_l^m(\Omega)-Y_l^{-m}(\Omega)]. \tag{2.1b}$$

Here and in the following, we work with real spherical harmonics and convention of Ref. 17. On the other hand, the symmetry lowering $Fm\bar{3}m\rightarrow Pa\bar{3}$ for UO_2 at T_N and $Fm\bar{3}m\rightarrow Pn\bar{3}m$ for NpO_2 at T_o is characterized by the appearance of triple-$\vec{q}$ antiferroquadrupolar order in the electronic density distribution at the actinide sites on the fcc lattice.

In real space, both space groups $Pa\bar{3}$ (No. 224, Ref. 18) and $Pn\bar{3}m$ (No. 205, Ref. 18) are characterized by the distribution of quadrupoles with specific orientations over four different sublattices with simple cubic structure. We label these sublattices which contain the sites (0,0,0) $(a/2)(0,1,1)$, $(a/2)(1,0,1)$, and $(a/2)(1,1,0)$ by $\{\vec{n}_p\}$, $p=1$–4, respectively. The most significant feature of the ordered phases is the existence of only one threefold axis of symmetry C_3 at each actinide site which is also a cube diagonal. The only quadrupole function compatible with the symmetry lowering is $Y_2^0(\Omega')$ in the coordinate system where the z' axis coincides with one of the threefold axes (cube diagonals): $[111]$, $[-1,-1,1]$, $[1,-1,-1]$, and $[-1,1,-1]$. Consequently, there are four such functions which are given by

$$\mathcal{S}_a(\Omega)=\frac{1}{\sqrt{3}}[Y_2^{1s}(\Omega)+Y_2^{1c}(\Omega)+Y_2^{2s}(\Omega)], \tag{2.2a}$$

$$\mathcal{S}_b(\Omega)=\frac{1}{\sqrt{3}}[-Y_2^{1s}(\Omega)-Y_2^{1c}(\Omega)+Y_2^{2s}(\Omega)], \tag{2.2b}$$

$$\mathcal{S}_c(\Omega)=\frac{1}{\sqrt{3}}[Y_2^{1s}(\Omega)-Y_2^{1c}(\Omega)-Y_2^{2s}(\Omega)], \tag{2.2c}$$

$$\mathcal{S}_d(\Omega)=\frac{1}{\sqrt{3}}[-Y_2^{1s}(\Omega)+Y_2^{1c}(\Omega)-Y_2^{2s}(\Omega)] \tag{2.2d}$$

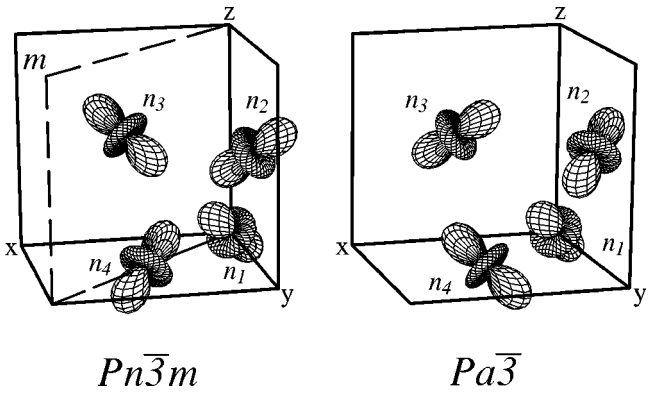

FIG. 1. $Pn\bar{3}m$ (NpO_2) and $Pa\bar{3}$ (UO_2) quadrupolar orderings. Both structures have the common S_6 (or $\bar{3}$) local site symmetry and belong to the rhombohedral (trigonal) system. They differ in the way the threefold axes and quadrupoles are distributed over four sublattices $\{n_p\}$, $p=1$–4 (see text for details). The $Pn\bar{3}m$ structure possesses three mirror planes one of which (m) is shown explicitly. The $Pa\bar{3}$ symmetry corresponds to domain I.

in the crystal fixed Cartesian system of axes. The spherical harmonics Y_2^{1s}, Y_2^{1c}, Y_2^{2s} belong to a three-dimensional irreducible representation T_{2g} of O_h. They are proportional to the Cartesian components yz, zx, and xy. We now distribute the four orientational functions S_a-S_d among the distinct sublattices $\{\vec{n}_p\}$, $p=1$–4. Keeping the threefold rotation symmetry about the $[111]$ axis and $\mathcal{S}_a$ for the first sublattice, we distinguish only three different choices here. The first is when (i) $\mathcal{S}_b$ corresponds to $\{\vec{n}_4\}$, $\mathcal{S}_c-\{\vec{n}_2\}$, and $\mathcal{S}_d-\{\vec{n}_3\}$. This gives the $Pn\bar{3}m$ structure, Fig. 1 left panel. The neptunium site symmetry is D_{3d}. Another assignment is (ii) $\mathcal{S}_b-\{\vec{n}_2\}$, $\mathcal{S}_c-\{\vec{n}_3\}$, and $\mathcal{S}_d-\{\vec{n}_4\}$. This scheme corresponds to the $Pa\bar{3}$ structure as shown in Fig. 1, right panel. The third choice is (iii) $\mathcal{S}_b-\{\vec{n}_3\}$, $\mathcal{S}_c-\{\vec{n}_4\}$, and $\mathcal{S}_d-\{\vec{n}_2\}$. This is simply another variant (or domain) of the $Pa\bar{3}$ structure. The uranium site symmetry is $S_6=C_3\times i$.

From the mathematical point of view, we are analyzing the symmetry lowering and the condensation schemes at the X point of the Brillouin zone (BZ) of the fcc lattice, which involves the density components of the T_{2g} symmetry. In both cases ($Pn\bar{3}m$ and $Pa\bar{3}$), the triple-$\vec{q}$ mode which drives the structural phase transition belongs to the X point of BZ $*\vec{q}^X$, and involves the three arms of the latter, $\vec{q}_x^X=(2\pi/a)(1,0,0)$, $\vec{q}_y^X=(2\pi/a)(0,1,0)$, and $\vec{q}_z^X=(2\pi/a)(0,0,1)$. To describe the three quadrupolar components $S_1=Y_2^{1s}$, $S_2=Y_2^{1c}$, $S_3=Y_2^{2s}$ at site $\vec{n}$, we introduce the functions $S_i(\vec{n})(i=1$–$3)$ and consider their Fourier transforms:

$$S_i(\vec{q})=\frac{1}{\sqrt{N}}\sum_{\vec{n}} e^{i\vec{q}\cdot\vec{X}(\vec{n})}S_i(\vec{n}), \tag{2.3}$$

where the position vector $\vec{X}$ runs over N sites of the face-centered-cubic neptunium lattice. The little group of $*\vec{q}^X$ is D_{4h} $(4/mmm)$. At $\vec{q}_x^X$ the functions S_2 and S_3 belong to the

E_g small representation, while the function S_1 belongs to the B_{2g} small representation. Consequently, we distinguish two different irreducible representations of the space group $Fm\bar{3}m$. The first one, X_5^+ in notations of Stokes and Hatch,[19] comprises six orientational functions, with two functions from every arm of $*\vec{q}^X$. The functions are $S_2(\vec{q}_x^X)$, $S_3(\vec{q}_x^X)$; $S_1(\vec{q}_y^X)$, $S_3(\vec{q}_y^X)$; $S_1(\vec{q}_z^X)$, and $S_2(\vec{q}_z^X)$. The second irreducible representation X_4^+ has only three components, with one function from each arm of $*\vec{q}^X$, namely, $S_1(\vec{q}_x^X)$, $S_2(\vec{q}_y^X)$, and $S_3(\vec{q}_z^X)$. For the symmetry lowering to the $Pa\bar{3}$ structure we obtain the following condensation scheme:

$$Fm\bar{3}m:X_5^+(\langle S_3(\vec{q}_x^X)\rangle=\langle S_1(\vec{q}_y^X)\rangle=\langle S_2(\vec{q}_z^X)\rangle=\rho_1\sqrt{N}\neq 0,$$

$$\langle S_2(\vec{q}_x^X)\rangle=\langle S_3(\vec{q}_y^X)\rangle=\langle S_1(\vec{q}_z^X)\rangle=0)$$

$$\rightarrow Pa\bar{3}(Z=4) \quad \text{domain I.} \tag{2.4}$$

Here $\langle \ldots \rangle$ stands for a quantum and thermal average and ρ_1 is the order-parameter amplitude. This condensation scheme corresponds to a domain shown in Fig. 1, and there are eight possible domains of $Pa\bar{3}$. In particular, there is a domain (iii) which we have already considered before ($\mathcal{S}_a-\{\vec{n}_1\}$, $\mathcal{S}_b-\{\vec{n}_3\}$, $\mathcal{S}_c-\{\vec{n}_4\}$, and $\mathcal{S}_d-\{\vec{n}_2\}$) when we analyzed the variants of distribution of $\mathcal{S}_a$–$\mathcal{S}_d$ over four sublattices. This domain is obtained as a result of the following symmetry breaking:

$$Fm\bar{3}m:X_5^+(\langle S_3(\vec{q}_x^X)\rangle=\langle S_1(\vec{q}_y^X)\rangle=\langle S_2(\vec{q}_z^X)\rangle=0,$$

$$\langle S_2(\vec{q}_x^X)\rangle=\langle S_3(\vec{q}_y^X)\rangle=\langle S_1(\vec{q}_z^X)\rangle=\rho_1\sqrt{N}\neq 0)$$

$$\rightarrow Pa\bar{3} \quad (Z=4) \quad \text{domain II.} \tag{2.5}$$

The X_5^+ active representation is defined by the star $\{\vec{k}_{10}\}$ and the loaded two-dimensional representation $\hat{\tau}^9$ in Kovalev's notation.[20]

The symmetry lowering for the $Pn\bar{3}m$ structure is described by

$$Fm\bar{3}m:X_4^+(\langle S_1(\vec{q}_x^X)\rangle=\langle S_2(\vec{q}_y^X)\rangle=\langle S_3(\vec{q}_z^X)\rangle=\rho_2\sqrt{N}\neq 0)$$

$$\rightarrow Pn\bar{3}m \quad (Z=4). \tag{2.6}$$

Here again ρ_2 is the order-parameter amplitude. The X_4^+ active representation corresponds to the irreducible star $\{\vec{k}_{10}\}$ and the loaded one-dimensional representation $\hat{\tau}^7$ in Kovalev's notation.[20] There are four domains for the $Pn\bar{3}m$ structure.

Although the two structures look similar there are two very important differences between them. First, as we have mentioned earlier, the $Pa\bar{3}$ structure allows for displacements of the oxygen sublattice, which can be understood in a simple way. Each uranium quadrupole of $Pa\bar{3}$ can be grouped with the two neighboring oxygen atoms lying on the correspondent main cube diagonal. For example, for the uranium atom at (0,0,0) (sublattice n_1 and the quadrupole alignment along the $\langle 111\rangle$ direction), these are oxygen atoms at $\pm a(1/4,1/4,1/4)$. In the low-temperature phase two oxygen atoms move towards the central uranium atom, as shown in Fig. 2. The same applies to three other sublattices of uranium. In NpO_2 such displacements are not possible. As follows from Fig. 1 for the $Pn\bar{3}m$ structure, four threefold axes of neighboring neptunium quadrupoles are intersected at one point, which is $a(1/4,1/4,1/4)$. A shift of oxygen from this position along one of the main diagonals (say, $\langle 111\rangle$) would destroy the threefold axial symmetry of other neighbors.

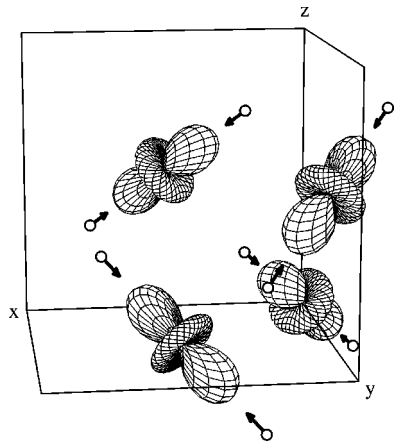

FIG. 2. Oxygen displacements of UO_2 in the $Pa\bar{3}$ structure.

Second, as we will show now, the $Pa\bar{3}$ order corresponds to an effective attraction among the quadrupoles on the fcc lattice while the $Pn\bar{3}m$ order results in a repulsion among them. We calculate the direct bilinear electronic quadrupole-quadrupole interaction on a fcc lattice.

We consider the quadrupolar components S_i of T_{2g} symmetry ($i=1$–3) at site $\vec{n}=0\equiv(0,0,0)(\vec{n}\in\{n_1\})$. There are 12 nearest neighbors of $\vec{n}$ belonging to three different sublattices $\{n_p\}$, $p=2$–4. The interactions between three components S_i centered at $\vec{n}=0$ and those (S_j) located at four nearest neighbors ($\vec{n}'=1$–4) of the second sublattice ($\vec{n}'\in\{n_2\}$) are given in Table I.

The matrix $S_i'(\vec{n})-S_j'(\vec{n}')$ for the fourth sublattice $\{n_4\}$ is given by the same table provided that the cyclic permutation $S_1\rightarrow S_3'$, $S_2\rightarrow S_1'$, $S_3\rightarrow S_2'$ is performed. Here we label four nearest neighbors $\vec{n}'=5$–8 of $\vec{n}$ as $5\equiv a(1/2,1/2,0)$, 6

TABLE I. The matrix of interaction $S_i(\vec{n})-S_j(\vec{n}')$ between three quadrupolar components of T_{2g} symmetry, $S_1=Y_2^{1s}$, $S_2=Y_2^{1c}$, $S_3=Y_2^{2s}$. S_i are centered at $\vec{n}=(0,0,0)$, S_j at four neighbors $\vec{n}'$ of the second sublattice $\{n_2\}$.

$\vec{n}'$	Coord.	$(i,j)=$	(1,1)	(2,2)	(3,3)	(1,2)	(1,3)	(2,3)
1	$a(0,\frac{1}{2},\frac{1}{2})$		γ	α	α	0	0	β
2	$a(0,-\frac{1}{2},\frac{1}{2})$		γ	α	α	0	0	$-\beta$
3	$a(0,-\frac{1}{2},-\frac{1}{2})$		γ	α	α	0	0	β
4	$a(0,\frac{1}{2},-\frac{1}{2})$		γ	α	α	0	0	$-\beta$

$\equiv a(-1/2,1/2,0)$, $7\equiv a(-1/2,-1/2,0)$, and $8\equiv a(1/2,-1/2,0)$. The matrix $S_i''(\vec{n})-S_j''(\vec{n}')$ for the third sublattice $\{n_3\}$ is obtained from Table I by replacing $S_1\rightarrow S_2''$, $S_2\rightarrow S_3''$, $S_3\rightarrow S_1''$. Here $\vec{n}'$ runs over the sites $9\equiv a(1/2,0,1/2)$, $10\equiv a(-1/2,0,1/2)$, $11\equiv a(-1/2,0,-1/2)$, and $12\equiv a(1/2,0,-1/2)$.

In real space the interaction potential of quadrupoles on fcc lattice sites is given by

$$V^{RR}=\frac{1}{2}\sum_{n}\sum_{n'}J_{ij}(\vec{n},\vec{n}')S_i(\vec{n})S_j(\vec{n}'), \qquad (2.7a)$$

where the elements of the interaction matrix $J(\vec{n},\vec{n}')$ follow from Table I and corresponding permutations. (The superscript R in V^{RR} stands for rotation, since the interaction depends on the instantaneous orientation of the quadrupoles. In analogy with the theory of molecular crystals we call this interaction a rotation-rotation interaction.) It is most convenient to write the quadrupolar interaction potential in Fourier space as

$$V^{RR}=\frac{1}{2}\sum_{\vec{q}}J_{ij}(\vec{q})S_i(\vec{q})S_j(-\vec{q}). \qquad (2.7b)$$

The interaction matrix is then given by

$$J(\vec{q})=4\begin{bmatrix}\gamma C_{yz}+\alpha(C_{zx}+C_{xy}) & -\beta S_{xy} & -\beta S_{zx}\\ -\beta S_{xy} & \gamma C_{zx}+\alpha(C_{xy}+C_{yz}) & -\beta S_{yz}\\ -\beta S_{zx} & -\beta S_{yz} & \gamma C_{xy}+\alpha(C_{yz}+C_{zx})\end{bmatrix}, \qquad (2.8)$$

where $C_{ij}=\cos(q_ia/2)\cos(q_ja/2)$ and $S_{ij}=\sin(q_ia/2)\sin(q_ja/2)$. The matrix $J(\vec{q})$ becomes diagonal at the X point of the Brillouin zone. For $\vec{q}=\vec{q}_x^X$, we have $J_{11}(\vec{q}_x^X)=4(\gamma-2\alpha)$, $J_{22}(\vec{q}_x^X)=J_{33}(\vec{q}_x^X)=-4\gamma$. We observe that $\gamma>0$, $\alpha<0$, independent of the lattice constant a. From the condensation scheme (2.4) for the $Pa\bar{3}$ structure, we then obtain that the interaction is maximum and attractive for the condensation of $S_3(\vec{q}_x^X)$. Similarly, $J_{11}(\vec{q}_y^X)=-4\gamma$ and $J_{22}(\vec{q}_z^X)=-4\gamma$ imply the condensation of $S_1(\vec{q}_y^X)$ and $S_2(\vec{q}_z^X)$, respectively. We conclude that the direct quadrupolar interaction on a fcc lattice stabilizes the $Pa\bar{3}$ structure. On the other hand, starting from the condensation scheme (2.6) of the $Pn\bar{3}m$ structure, we find $J_{11}(\vec{q}_x^X)=J_{22}(\vec{q}_y^X)=J_{33}(\vec{q}_z^X)=4(\gamma-2\alpha)>0$, which is repulsive. Hence, the $Pn\bar{3}m$ structure cannot be stabilized solely by the direct electric quadrupole interaction. The fact that the quadrupolar interaction is attractive for the $Pa\bar{3}$ structure (and repulsive for $Pn\bar{3}m$) is the reason why $Pa\bar{3}$ (and not $Pn\bar{3}m$) is found in many molecular solids with quadrupolar interactions such as H_2 (Ref. 21), N_2 (Ref. 22), NaO_2 (Ref. 23).

In fact, on a fcc lattice, the structure of the interaction matrix (2.8) and the condensation scheme (2.4) is not restricted to quadrupolar ($l=2$) interactions, but applies to order-parameter variables of even l multipoles that transform as the three components of an irreducible representation T_{2g} of the cubic point group O_h. The most prominent example is solid C_{60},[24,25] where the orientationally ordered phase has $Pa\bar{3}$ structure. Here the icosahedral symmetry imposes $l=6,10,\ldots$, and the expressions of the condensation scheme and of the multipolar interactions are of forms (2.4) and (2.8), respectively.[26]

From the above discussion of the condensation schemes and interactions, we conclude that in order to explain the $Pn\bar{3}m$ structure of NpO_2 one should resort to indirect oxygen mediated (superexchange[27]) interactions between Np electric quadrupoles.

This conclusion is further supported by a calculation of the coupling of the quadrupoles to phonons. By studying the interaction of quadrupoles on a deformable lattice, we found that the direct electric quadrupole-quadrupole interaction in NpO_2 leads to an expansion of the cubic lattice, which is in contradiction with the experiment. Hence, we conclude in agreement with Refs. 13 and 14 that the direct quadrupole-quadrupole interaction is not the driving mechanism for the $Pn\bar{3}m$ structure and the oxygen-mediated interactions are important for this compound.

III. RXS AND DOMAIN STRUCTURE

Now we will study how the $Pn\bar{3}m$ and $Pa\bar{3}$ structures manifest themselves in resonant x-ray scattering experiments.[28,14] The tensor of scattering on the quadrupolar density of a neptunium atom in a cubic lattice is given by[29–31]

$$\hat{f}_n=\tilde{f}\begin{pmatrix}0 & \rho_1 & \rho_2\\ \rho_1 & 0 & \rho_3\\ \rho_2 & \rho_3 & 0\end{pmatrix}, \qquad (3.1)$$

where $\rho_i=\pm 1$. We have the following correspondence[30,31] between the functions $\mathcal{S}_n$, Eqs. (2.2a)–(2.2d), and the scattering tensors: the function $\mathcal{S}_a$ corresponds to $\hat{f}_a$, where $\rho_1=\rho_2=\rho_3=1$, the function $\mathcal{S}_b$ to $\hat{f}_b$ with $\rho_1=1$, $\rho_2=\rho_3=-1$; the function $\mathcal{S}_c$ to $\hat{f}_c$ with $\rho_1=\rho_2=-1$, $\rho_3=1$; and

TABLE II. Tensor $\mathcal{F}(h,k,l)=\tilde{F}\mathcal{M}$ for the superstructure Bragg reflections on quadrupolar densities of Np. $\mathcal{M}=A,B$ or C, Eq. (3.4), I (ii) and II (iii) refer to two domains of the $Pa\bar{3}$ structure described in the text, 0 is the zero matrix.

Bragg reflection	$Pn\bar{3}m$	$Pa\bar{3}$	
h,k,l:	(i)	I (ii)	II (iii)
$h,k,l=2n$	0	0	0
$h,k,l=2n+1$	0	0	0
$h=2n+1,\ k,l=2n$	A	C	B
$k=2n+1,\ h,l=2n$	B	A	C
$l=2n+1,\ h,k=2n$	C	B	A
$h,k=2n+1,\ l=2n$	C	B	A
$h,l=2n+1,\ k=2n$	B	A	C
$k,l=2n+1,\ h=2n$	A	C	B

$\mathcal{S}_d$ to $\hat{f}_d$ with $\rho_1=\rho_3=-1,\ \rho_2=1$. The scattering tensor structure amplitude is found as

$$\mathcal{F}(h,k,l)=\sum_{n=1}^{N}\hat{f}_n e^{i\vec{K}\cdot\vec{X}(n)}, \tag{3.2}$$

where $\vec{K}=(2\pi/a)(h,k,l)$ stands for the vectors of the reciprocal lattice and a is the cubic lattice constant. In performing the summation in Eq. (3.2) we distinguish four contributions from four sublattices $\{n_p\}$, $p=1$–4. We are mainly interested in superstructure Bragg reflections. We obtain then that, in general,

$$\mathcal{F}(h,k,l)=\tilde{F}\mathcal{M}, \tag{3.3}$$

where $\tilde{F}=\tilde{f}N$ and the matrix $\mathcal{M}$ is either A, B, or C:

$$A=\begin{pmatrix}0&0&0\\0&0&1\\0&1&0\end{pmatrix},\quad B=\begin{pmatrix}0&0&1\\0&0&0\\1&0&0\end{pmatrix},\quad C=\begin{pmatrix}0&1&0\\1&0&0\\0&0&0\end{pmatrix}. \tag{3.4}$$

In Table II we quote which of the matrices (A,B,C) occurs for every particular case of (h,k,l) for the $Pn\bar{3}m$ and $Pa\bar{3}$ structures. We recall that the conditions[18] for the isotropic scattering on the fcc lattice of Np (from the spherically symmetric densities) are $h+k,k+l=2n$, which corresponds to two first lines of Table II.

Finally, we consider the polarization dependencies for resonant x-ray scattering experiments. We assume that a crystal has a flat (001) surface and the azimuthal angle ψ is counted from the x axis defined by $\vec{e}_x=(1,0,0)$.[14] The incident beam direction is given by $(-\cos\Theta\cos\psi,\ -\cos\Theta\sin\psi,\ -\sin\Theta)$, and the scattered beam direction by $(-\cos\Theta\cos\psi,\ -\cos\Theta\sin\psi,\ \sin\Theta)$. We introduce the standard polarization vectors $\vec{e}_i(i=1$–$3)$ parallel $(\vec{\pi}_i,\ \vec{\pi}_f)$ or perpendicular $(\vec{\sigma})$ to the scattered plane,

TABLE III. The structure-factor amplitudes $F_{p\to p'}(h,k,l)/\tilde{F}$ for four polarization channels of RXS and the matrices A, B, and C.

$p\to p'$	A	B	C
$\sigma\to\sigma$	0	0	$-\sin(2\psi)$
$\sigma\to\pi_f$	$\cos\Theta\cos\psi$	$-\cos\Theta\sin\psi$	$\cos(2\psi)\sin\Theta$
$\pi_i\to\sigma$	$\cos\Theta\cos\psi$	$-\cos\Theta\sin\psi$	$-\cos(2\psi)\sin\Theta$
$\pi_i\to\pi_f$	0	0	$\sin(2\psi)\sin^2\Theta$

$$\vec{\sigma}=(-\sin\psi,\cos\psi,0), \tag{3.5a}$$

$$\vec{\pi}_i=(-\sin\Theta\cos\psi,-\sin\Theta\sin\psi,\cos\Theta), \tag{3.5b}$$

$$\vec{\pi}_f=(\sin\Theta\cos\psi,\sin\Theta\sin\psi,\cos\Theta). \tag{3.5c}$$

A structure-factor amplitude $F(h,k,l)$ is found as[29–31]

$$F_{p\to p'}(h,k,l)=\tilde{F}\vec{e}^{\,T}_{p'}\mathcal{M}\vec{e}_p, \tag{3.6}$$

where T stands for transpose and $p\to p'$ denotes one of the four polarization channels, $\sigma\to\sigma$, $\sigma\to\pi_f$, $\pi_i\to\sigma$, and $\pi_i\to\pi_f$. The structure-factor amplitudes for the three cases $(\mathcal{M}=A,B,C)$ are quoted in Table III. The corresponding intensities of the superstructure Bragg reflections are found as $I_{p\to p'}(h,k,l)=|F_{p\to p'}(h,k,l)|^2$.

From Tables II and III one can easily obtain all necessary dependencies for intensities of different polarizations. For example, the intensity of the (003) reflection of $Pn\bar{3}m$ is exactly the same as the intensity of the same polarization of the (300) reflection of domain I (ii) of $Pa\bar{3}$, and the intensity of the (030) reflection of domain II (iii) of $Pa\bar{3}$. Furthermore, the (013) reflection of domain I (ii), and the (103) reflection of domain II (iii) of $Pa\bar{3}$ also have the same intensity, and so on. Since both symmetries are very similar, we believe that special care should be taken to discriminate between the $Pn\bar{3}m$ and $Pa\bar{3}$ structures.

Tables II and III are also useful in considering the contributions from the domains of the same group. If the domain sizes are larger than the coherence length of the x rays, then the effect of domains is reduced to averaging over the corresponding intensities, which is a trivial task. However, the tendency in recent synchrotron experiments is towards more perfect and collimated beams and larger coherence lengths. This implies, especially for the relatively soft x rays at the actinide M edges, that the average should be taken over amplitudes rather than intensities.[32] Our analysis below is given for such a case of coherent scattering on the crystal domains.

We start with the $Pn\bar{3}m$ structure. The four domains differ by the orientation of the $Y_2^0(\Omega')$ quadrupolar function at $\vec{n}=0$. This function may be chosen to align along four main cube diagonals, which are connected with each other through rotations by $\pi/2$ about the z axis. Hence, all four domains are obtained from the first (i) by applying three consecutive ro-

tations by $\pi/2$ about the z axis. The effect of the domains in RXS experiments is equivalent to a superposition of four structure amplitudes, Table III, with angles ψ, $\psi+\pi/2$, $\psi+\pi$, and $\psi+3\pi/2$. We label these domains by indices $d1-d4$, and introduce their populations $P_{d1}-P_{d4}$. The population of a domain d is defined as $P_d=N_d/N$, where N_d is the total number of neptunium atoms in the domain. Then we obtain from Eq. (3.6) that the structure amplitude for the $\sigma\rightarrow\sigma$ and $\sigma\rightarrow\pi_f$ channels of the (003) reflection is given by

$$F_{\sigma\rightarrow\sigma}(003)=-\tilde{F}\tilde{P}\sin(2\psi), \tag{3.7a}$$

$$F_{\sigma\rightarrow\pi_f}(003)=\tilde{F}\tilde{P}\cos(2\psi)\sin\Theta, \tag{3.7b}$$

where

$$\tilde{P}=(P_{d1}-P_{d2}+P_{d3}-P_{d4}). \tag{3.7c}$$

If $P_{d1}+P_{d3}=P_{d2}+P_{d4}$, $\tilde{P}=0$ and the (003) Bragg reflection is suppressed. Otherwise, the ψ and Θ dependencies in Eqs. (3.7a) and (3.7b) are exactly the same as for a single domain, Tables II, III. For the (300) reflection of $Pn\bar{3}m$ one obtains that

$$F_{\sigma\rightarrow\pi_f}(300)=\tilde{F}P'\cos\Theta\cos(\psi+\psi_0), \tag{3.8a}$$

where

$$\psi_0=\arccos([P_{d1}-P_{d3}]/P'), \tag{3.8b}$$

$$P'=\sqrt{[P_{d1}-P_{d3}]^2+[P_{d2}-P_{d4}]^2}. \tag{3.8c}$$

Comparing this result with the expression for a single domain, we observe that the main effect is the phase shift ψ_0 given by Eq. (3.8b). The condition for suppression of the reflection is $P_{d1}=P_{d3}$ and $P_{d2}=P_{d4}$. The polarization dependencies of the other reflections of $Pn\bar{3}m$ can be figured out analogously.

There are eight domains of $Pa\bar{3}$ structure. Earlier we have already considered the two basic variants of $Pa\bar{3}$: I (ii) and II (iii). The others are obtained by rotating these two variants by the angles $\pi/2$, π, and $3\pi/2$ about the z axis. Applying the rotations to I and II, we arrive at two series. We label the population of the series of domains by the indices $P^I_{d1}-P^I_{d4}$, and $P^{II}_{d1}-P^{II}_{d4}$, respectively. The two series result in two distinct scattering matrices, for example, for (003) they are B and A, for (300) C and B, etc., see Table II. The domain pattern produces a superposition of eight terms (amplitudes). Each term corresponds to one of the two matrices and to one of the four azimuthal angles: ψ, $\psi+\pi/2$, $\psi+\pi$, and $\psi+3\pi/2$. The relevant expressions are obtained in the same way which we have used to derive Eqs. (3.7a)–(3.7c) and (3.8a)–(3.8c). For example,

$$F_{\sigma\rightarrow\pi_f}(003)=0, \tag{3.9a}$$

$$F_{\sigma\rightarrow\pi_f}(003)=\tilde{F}\cos\Theta(-P'^{I}\sin(\psi+\psi_0^I)+P'^{II}\cos(\psi+\psi_0^{II})), \tag{3.9b}$$

The latter expression can be transformed to a shifted sin- or cos- like functions, i.e., $F_{\sigma\rightarrow\pi_f}(003)\sim\cos\Theta\sin(\psi+\psi_0')$, where ψ_0' is a phase shift depending on the domain pattern of $Pa\bar{3}$. P'^{I}, P'^{II}, and ψ_0^I, ψ_0^{II} are given by Eqs. (3.8c) and (3.8b), where P_{di} $(i=1-4)$ are replaced by P^I_{di} or P^{II}_{di}. For the (300) reflection of $Pa\bar{3}$, we find

$$F_{\sigma\rightarrow\sigma}(300)=-\tilde{F}\tilde{P}^I\sin(2\psi), \tag{3.10a}$$

$$F_{\sigma\rightarrow\pi_f}(300)=\tilde{F}\tilde{P}^I\cos(2\psi)\sin\Theta-\tilde{F}P'^{II}\sin(\psi+\psi_0^{II})\cos\Theta. \tag{3.10b}$$

Here, again $\tilde{P}^I$ is given by Eq. (3.7c) for P^I_{di}, $i=1-4$. As before, the superstructure Bragg reflections are suppressed in the case of equal population of eight domains in the crystal.

IV. CONCLUSIONS

In resonant x-ray scattering experiments the transition to the ordered phase at $T_o=25.5$ K in NpO_2 manifests itself by the appearance of superstructure Bragg reflections [such as (003) and others], which are not compatible with the $Fm\bar{3}m$ structure of the disordered phase.[9,14] Paixão *et al.*,[14] ascribed the symmetry of the ordered phase to the $Pn\bar{3}m$ space group (No. 224, Ref. 18). In this work we have derived the symmetry lowering scheme for the phase transition, Eq. (2.6). The active mode is X_4^+ in notations of Stokes and Hatch[19] and $\hat{\tau}^7$ in Kovalev's notation.[20] It involves three quadrupolar components of the cubic T_{2g} (or Γ_5) symmetry. At low temperatures, the space symmetry is again cubic but there are four different sublattices which are characterized by four different orientations of the neptunium electronic quadrupole, Fig. 1.

Besides $Pn\bar{3}m$, we discuss also the space group $Pa\bar{3}$ (No. 205, Ref. 18), which is another variant of the triple-$\vec{q}^X$ quadrupole ordering. This structure is realized for uranium quadrupoles of UO_2. $Pn\bar{3}m$ and $Pa\bar{3}$ are close symmetries. They imply condensations of different modes (X_4^+ and X_5^+, Ref. 19) at the same $X-$point of the Brillouin zone and differ in the way the threefold axes of symmetry are distributed over various $\langle 111\rangle$ directions, Fig. 1. In both cases the actinide site symmetry at low T is rhombohedral (trigonal). We have shown that the two structures are different with respect to the direct bilinear quadrupole-quadrupole interactions. The $Pa\bar{3}$ structure leads to an attraction between the quadrupoles, while the $Pn\bar{3}m$ symmetry implies a repulsion. We then conclude that the direct bilinear quadrupole-quadrupole interaction is not the leading one and that the oxygen mediated interactions play an important role in these dioxides. This oxygen mediated interaction results in different space symmetries and condensation schemes for NpO_2 and UO_2. Correspondingly, the oxygen site symmetry is different. In NpO_2 below T_o oxygen remains tetrahedrally

coordinated while in the ordered phase of UO_2 one uranium-oxygen bond strengthens at the expense of three others, see Fig. 2.

We have considered the dependence of the scattering amplitude for different polarizations on the azimuthal angle ψ and the Bragg angle Θ taking into account the domain pattern of both symmetries. $Pn\bar{3}m$ and $Pa\bar{3}$ produce superstructure Bragg reflections at the same sites (h,k,l) of the reciprocal lattice (Tables II and III). The relation between the space groups is such that in RXS experiments, the (00ℓ) reflection of $Pn\bar{3}m$ behaves like the $(\ell 00)$ and $(0\ell 0)$ reflections of $Pa\bar{3}$ $(\ell=2n+1)$.

The interesting questions posed by the hidden symmetry change in NpO_2 are whether the same mechanism occurs in other cubic crystals [cerium (Refs. 10,11), $YbInCu_4$ (Ref. 12)] where ''isostructural'' phase transitions are accompanied by a loss of magnetic moments, and how magnetic and structural properties are interconnected.[16] The issue is far from complete understanding and we believe that further experimental and theoretical works are needed to clarify it.

ACKNOWLEDGMENTS

We acknowledge illuminating discussions with C. Detlefs, P. Santini and the authors of Ref. 14 on this problem. This work has been financially supported by the Fonds voor Wetenschappelijk Onderzoek, Vlaanderen.

*Also at: Institute of Physical Chemistry of RAS, Leninskii prospect 31, 117915 Moscow, Russia.

[1] E.F. Westrum, J.B. Hatcher, and D.W. Osborne, J. Chem. Phys. **21**, 419 (1953); D.W. Osborne and E.F. Westrum, *ibid.* **21**, 1884 (1953).

[2] P. Erdös and J. Robinson, *The Physics of Actinide Compounds* (Plenum Press, New York, 1983).

[3] P. Santini, R. Lémanski, and P. Erdös, Adv. Phys. **48**, 537 (1999).

[4] B.C. Frazer, G. Shirane, D.E. Cox, and C.E. Olsen, Phys. Rev. **140**, A1448 (1965); B.T.M. Willis and R.I. Taylor, Phys. Lett. **17**, 188 (1965).

[5] R. Caciuffo, G. Amoretti, P. Santini, G.H. Lander, J. Kulda, and P. de V. Du Plessis, Phys. Rev. B **59**, 13 892 (1999).

[6] P. Erdös, G. Solt, Z. Zolnierek, A. Blaise, and J.M. Fournier, Physica **102B**, 164 (1980).

[7] B.D. Dunlap, G.M. Kalvius, D.J. Lam, and M.B. Brodsky, J. Phys. Chem. Solids **29**, 1365 (1968); R. Caciuffo, G.H. Lander, J.C. Spirlet, J.M. Fournier, and W.F. Kuhs, Solid State Commun. **64**, 149 (1987), and references on earlier work on neutron diffraction there.

[8] J. Faber and G.H. Lander, Phys. Rev. B **14**, 1151 (1976).

[9] D. Mannix, G.H. Lander, J. Rebizant, R. Caciuffo, N. Bernhoeft, E. Lidström, and C. Vettier, Phys. Rev. B **60**, 15 187 (1999).

[10] D.C. Koskenmaki and K.A. Gschneidner, Jr., *Handbook on the Physics and Chemistry of Rare Earths*, edited by K.A. Gschneidner, Jr. and L. Eyring (North-Holland, Amsterdam, 1978), p. 337.

[11] D. Malterre, M. Grioni, and Y. Baer, Adv. Phys. **45**, 299 (1996).

[12] J.L. Sarrao, Physica B **259-261**, 128 (1999), and references therein.

[13] P. Santini and G. Amoretti, Phys. Rev. Lett. **85**, 2188 (2000).

[14] J.A. Paixão, C. Detlefs, M.J. Longfield, R. Caciuffo, P. Santini, N. Bernhoeft, J. Rabizant, and G.H. Lander, Phys. Rev. Lett. **89**, 187202 (2002).

[15] W. Kopmann, F.J. Litterst, H-H. Klauss, M. Hillberg, W. Wagener, G.M. Kalvius, E. Schreier, F.J. Burghart, J. Rebizant, and G.H. Lander, J. Alloys Compd. **271-273**, 463 (1998).

[16] A.V. Nikolaev and K.H. Michel, Eur. Phys. J. B **9**, 619 (1999); **17**, 363 (2000); A.V. Nikolaev and K.H. Michel, Phys. Rev. B **66**, 054103 (2002).

[17] C.J. Bradley and A.P. Cracknell, *The Mathematical Theory of Symmetry in Solids* (Clarendon, Oxford, 1972).

[18] *International Tables for Crystallography*, edited by Theo Hahn (Reidel, Boston, 1983), Vol. 4.

[19] H.T. Stokes and D.M. Hatch, *Isotropy Subgroups of the 230 Crystallographic Space Groups* (World Scientific, Singapore, 1988).

[20] O.V. Kovalev, *Irreducible Representations of the Space Groups* (Gordon and Breach, New York, 1965).

[21] J. Van Kranendonk, *Solid Hydrogen* (Plenum Press, New York, 1983).

[22] T.A. Scott, Phys. Rep. **27**, 89 (1976).

[23] P. Zielinski and K. Parlinski, J. Phys. C **17**, 3287 (1984).

[24] R. Sachidanandam and A.B. Harris, Phys. Rev. Lett. **67**, 1467 (1991); P.A. Heiney, J.E. Fischer, A.R. McGhie, W.J. Romanow, A.M. Denenstein, J.P. McCauley, Jr., and A.B. Smith III, *ibid.* **67**, 1468 (1991).

[25] W.I.F. David, R.M. Ibberson, J.C. Matthewman, K. Prassides, T.J.S. Dennis, J.P. Hare, H.W. Kroto, and D.R.M. Walton, Nature (London) **353**, 147 (1991).

[26] K.H. Michel, J.R.D. Copley, and D.A. Neumann, Phys. Rev. Lett. **68**, 2929 (1992); K.H. Michel, Z. Phys. B: Condens. Matter **88**, 71 (1992).

[27] P.W. Anderson, Phys. Rev. **79**, 350 (1950); **115**, 2 (1959).

[28] D.H. Templeton and L.K. Templeton, Acta Crystallogr., Sect. A: Cryst. Phys., Diffr., Theor. Gen. Crystallogr. **36**, 237 (1980).

[29] V.E. Dmitrienko, Acta Crystallogr., Sect. A: Cryst. Phys., Diffr., Theor. Gen. Crystallogr. **39**, 29 (1983).

[30] V.E. Dmitrienko, Acta Crystallogr., Sect. A: Cryst. Phys., Diffr., Theor. Gen. Crystallogr. **40**, 89 (1984).

[31] D.H. Templeton and L.K. Templeton, Acta Crystallogr., Sect. A: Cryst. Phys., Diffr., Theor. Gen. Crystallogr. **42**, 478 (1986).

[32] C. Detlefs (private communication).